Astronomy & Astrophysics

First stars

XV. Third-peak *r*-process element and actinide abundances in the uranium-rich star CS31082-001[*]

B. Barbuy[1], M. Spite[2], V. Hill[3], F. Primas[4], B. Plez[5], R. Cayrel[2], F. Spite[2], S. Wanajo[6,7], C. Siqueira Mello Jr.[1], J. Andersen[8,9], B. Nordström[8], T. C. Beers[10], P. Bonifacio[2], P. François[2], and P. Molaro[11]

[1] Universidade de São Paulo, IAG, Rua do Matão 1226, Cidade Universitária, São Paulo 05508-900, Brazil
e-mail: barbuy@astro.iag.usp.br
[2] GEPI, Observatoire de Paris, CNRS, UMR 8111, 92195 Meudon Cedex, France
[3] Université de Sophia-Antipolis, Observatoire de la Côte d'Azur, CNRS UMR 6202, BP 4229, 06304 Nice Cedex 4, France
[4] European Southern Observatory, Karl Schwarzschild Strasse 2, 85748 Garching bei München, Germany
[5] LUPM, CNRS, UMR 5299, Université de Montpellier II, 34095 Montpellier Cedex 05, France
[6] Technische Universität München, Excellence Cluster Universe, Boltzmannstr. 2, 85748 Garching, Germany
[7] Max-Planck-Institut für Astrophysik, Karl-Schwarzschild-Str. 1, 85748 Garching, Germany
[8] The Niels Bohr Institute, Juliane Maries Vej 30, 2100 Copenhagen, Denmark
[9] Nordic Optical Telescope, Apartado 474, 38700 Santa Cruz de La Palma, Spain
[10] Michigan State University, Department of Physics & Astronomy, and JINA: Joinst Institute for Nuclear Physics, East Lansing, MI 48824, USA
[11] INAF – Osservatorio Astronomico di Trieste, via Tiepolo 11, 34143 Trieste, Italy

ABSTRACT

Context. A small fraction of extremely metal-poor (EMP) stars exhibit moderate to extreme excesses of heavy neutron-capture elements produced in the *r*-process. The production site(s) of these elements in the early Galaxy remain(s) unclear, as is the reason for their occasional enhancement in the otherwise regular pattern of abundances of elements up to the iron peak. The detailed abundance pattern of the heaviest elements in EMP stars provides insight into their origin and role in the chemical enrichment of the early Galaxy and in radioactive nucleochronology.
Aims. The EMP giant star CS 31082-001 ([Fe/H] $\sim$ −2.9) exhibits an extreme enhancement of neutron-capture elements ([r/Fe] $\sim$ +1.7) with U and Th enhanced by a further $\sim$+0.7 dex, and a minimum of blending by molecular lines such as CH or CN. A rich inventory of *r*-process element abundances was established previously from optical spectra. Here we aim to supplement these data with abundances from near-UV spectroscopy of the third-peak neutron-capture elements, which are crucial for understanding the synthesis of the heaviest elements.
Methods. Near-UV spectra from HST/STIS were analysed with LTE model atmospheres and spectrum synthesis calculations to derive new abundances of Os, Ir, Pt, Au, Bi and Pb in CS 31082-001.
Results. Together with earlier data, the resulting abundance pattern for the *r*-process elements provides improved constraints on the nature of the *r*-process. The observed U and Th abundances and the initial production ratio place CS 31082-001 as one of the oldest stars in the Galaxy, consistent with its extreme metal deficiency. Comparison with the heaviest stable reference elements and with the daughter nuclides Pb and Bi provides a consistency check on this age determination. Finally, the existence of such *r*-element rich stars indicate that the early chemical evolution of the Galaxy was localised and inhomogeneous.

Key words. stars: abundances – Galaxy: halo – galaxies: abundances – stars: Population II – stars: individual: BPS CS 31082-001

1. Introduction

A small fraction of extremely metal-poor stars ([Fe/H] < −3; EMP stars) in the Galactic halo shows enrichment in heavy neutron-capture elements. The abundance pattern of these elements is assumed to have an origin through a rapid neutron capture, the *r*-process, since the observed abundance pattern is generally indistinguishable from that of the *r*-process nuclei in the Solar System (except for Th and U). Their overall abundance level relative to iron is enhanced by factors between 2 and 10 (the r-I stars) or higher (10-80; r-II stars; Beers & Christlieb 2005). *s*-process elements are not expected to be present at such low metallicities, except if due to mass transfer from an AGB binary companion where they are produced.

These stars, and the more numerous stars with strong carbon enhancements (CEMP stars), raise two important questions about the production of and enrichment by heavy elements in the early Galaxy: *(i)* what were the production sites? and *(ii)* what processes of local heavy-element production, mixing and enrichment in the early Galaxy could produce certain element combinations in very uniform proportions in parallel with occasional large excesses of other classes of elements?

This paper aims to improve our understanding of one of the cleanest examples of extreme *r*-element enhancement. For

---

[*] Based on observations made with the NASA/ESA Hubble Space Telescope (HST) through the Space Telescope Science Institute, operated by the Association of Universities for Research in Astronomy, Inc., under NASA contract NAS5-26555; and with the ESO Very Large Telescope at Paranal Observatory, Chile; Progr. ID 165.N-0276.

clarity, these elements are grouped in first-peak ($38 \leq Z \leq 48$), second-peak ($56 \leq Z \leq 72$, including the rare earths) and third-peak elements ($76 \leq Z \leq 88$), and the actinides ($Z \geq 89$). The heaviest elements are our primary concern here.

The site(s) of *r*-element production is/are still not known with any certainty (e.g. Wanajo & Ishimaru 2006; Kratz et al. 2007; Thielemann et al. 2010). The most promising recent models involve high-entropy neutrino-driven winds of neutron-rich matter, which build up heavy nuclei near the neutrino sphere of a core-collapse supernova (Woosley et al. 1994; Wanajo 2007 and references therein). Studies of the Galactic chemical evolution also support core-collapse supernovae, in particular near their low mass end (∼8–10 $M_\odot$), as the dominant source of r-process elements (e.g. Mathews & Cowan 1990; Ishimaru & Wanajo 1999).

However, the latest hydrodynamical simulations with accurate neutrino transport (Fischer et al. 2010; Hüdepohl 2010) show that neutrino winds are proton-rich, not neutron-rich as found in some older simulations (Woosley et al. 1994). This makes the neutrino wind scenario for the origin of the heavy r-process elements doubtful. Wanajo et al. (2011) also show that low mass O-Ne-Mg (electron-capture) supernovae might produce the weak r-elements, but no heavier than $A \sim 120$. As plausible alternatives, neutron-rich ejecta from neutron star-neutron star (NS-NS) or black hole-neutron star (BH-NS) binary mergers have been suggested to be the astrophysical sites of the main r-process (Lattimer et al. 1977; Meyer 1989; Freiburghaus et al. 1999; Surnam et al. 2008; Wanajo & Janka 2011; Goriely et al. 2011). However the role of compact object mergers is controversial. Argast et al. (2004) claim that current merger models cannot fit the abundance data for metal-poor stars (but see De Donder & Vanbeveren 2004). In contrast, Prantzos (2006) suggests that mergers cannot be excluded as the predominant r-process origin in the framework of hierarchical clustering of sub-halos to the Galactic Halo system.

Detailed abundances of the elements produced by *r*-process nucleosynthesis in various circumstances are our best observational clues to their nature. These abundances are known in great detail in the Solar System, but represent the integrated result of nucleosynthesis in many generations of stars. A cleaner picture can be obtained by considering the products of heavy-element production in the first generation(s) of stars, as recorded in the low-mass stars that survive until today.

This paper presents an abundance analysis of the third-peak neutron-capture elements in the extremely *r*-element-rich EMP star CS 31082-001. We derive abundances of Os, Ir, Pt and Au as well as the decay products Bi and Pb of the long-lived radioactive elements Th and U, based on new HST/STIS spectra and our earlier ground-based VLT/UVES data.

Section 2 summarises the salient characteristics of the three most extreme *r*-element enhanced stars known. Section 3 describes our new spectroscopic observations and Sect. 4 the determination of heavy-element abundances in CS 31082-001. Section 5 discusses the use of different radioactive chronometer pairs to better understand the *r*-process and to derive the age of CS 31082-001, while Sect. 6 summarises our conclusions.

2. The *r*-element-rich EMP stars and the actinides

Beers & Christlieb 2005 classified the *r*-element enriched EMP stars as r-I or r-II stars according to the dominantly r-process element Europium abundance ($0.3 <$ [Eu/Fe] < 1.0 or [Eu/Fe] > 1.0, respectively); thus, a continuum of *r*-element enhancement

factors exists among EMP stars. A low Barium abundance ([Ba/Eu] < 0) is also required (Ba is mainly an *s*-process element).

It is important to note that the *r*-element abundance pattern is identical in all the known *r*-process enhanced stars, from the rare earths to the third *r*-process peak (Roederer et al. 2009). However, Th is further enhanced relative to this pattern in four stars: CS 31082-001, CS 30306-132 (Honda et al. 2004), CS 31078-018 (Lai et al. 2008) and HE 1219-0312 (Hayek et al. 2009) – the so-called "actinide boost". In these stars, the actinides clearly had a different nucleosynthesis history than the stable third-peak elements.

So far, 12 EMP r-II giant stars are known (Hayek et al. 2009); six of these have well-determined Th abundances, and two have U detections as well: CS 31082-001 (Hill et al. 2002) and HE 1523-0901 (Frebel et al. 2007). Recently, a dwarf star has been added to the list of r-enhanced stars, SDSS J2357−0052 (Aoki et al. 2010). The classification by Beers & Christlieb (2005) does not strictly apply to the four most r-element enhanced stars, given that they show [Ba/Fe] > 0 (in fact [Ba/Fe] $\gtrsim 1.0$), instead of [Ba/Fe] < 0. Nevertheless, the notation is designed to indicate that the Ba abundance, taken as representative of s-process elements, is far reduced from its normal s-process dominated value, relative to that of the almost pure r-element Eu. This condition does apply in terms of [Ba/Eu] $= -0.65$ for CS 22892-052 (Sneden et al. 2008), -0.46 for CS 31082-001 (Hill et al. 2002), -3.24 for HE 1523-0901 (Frebel et al. 2008, computed with 3D model atmospheres), and -0.80 for SDSS J2357-0052 (Aoki et al. 2010).

The three most extreme r-element enhanced giants have attracted the greatest attention, and their abundance patterns have been studied in very considerable detail, notably with reference to the prospects for radioactive age determinations. Their history is briefly summarised here.

CS 22892-052 ($T_{\rm eff} = 4760$ K, $\log g = 1.3$, [Fe/H] $= -3.1$, $V = 13.2$) has been studied extensively from the ground (e.g., McWilliam et al. 1995; Sneden et al. 1996, 2000, 2003; Cowan et al. 2005; Cowan & Sneden 2006), and also in the near-UV by Cowan et al. (2005) in order to study the heaviest neutron-capture elements that are only accessible from space. The overall *r*-process enhancement is [r/Fe] $\sim +1.7$ dex. Th is also strong, but a CN line masks the single U II line at 3859.6 Å due to a carbon enhancement of [C/Fe] $\sim +1.0$, so only an upper limit to the U abundance is available.

CS 31082-001 ($T_{\rm eff} = 4825$ K, $\log g = 1.5$, [Fe/H] $= -2.9$, $V = 11.7$) is 1.5 mag brighter than CS 22892-052 and has a similar [r/Fe] $\sim +1.7$, but [C/Fe] ~ 0.0. Both Th and U exhibit a large "actinide boost" of $\sim+0.7$ dex relative to the general *r*-process level. Hence, the present-day Th abundance in CS 31082-001 is larger than the average for a Solar System third-peak element despite ∼14 Gyr of radioactive decay, and the U II line at 3859.6 Å is readily measurable (Cayrel et al. 2001; Hill et al. 2001, 2002).

HE 1523-0901 ($T_{\rm eff} = 4630$ K, $\log g = 1.0$, [Fe/H] $= -2.95$, $V = 11.1$; Frebel et al. 2007) is the brightest and most recently discovered of the three stars. It shows a similar *r*-element enhancement of [r/Fe] $\sim+1.8$ dex, including Th and U; i.e. *no* "actinide boost" is present in this star. [C/Fe] ~ -0.3, so the U II line is also measurable in HE 1523-0901, and the decay of U relative to both Th and several stable heavy reference elements yields consistent age estimates.

The star CS 22183-031 at [Fe/H] $= -2.93$ and [r/Fe] $= +1.2$ (Honda et al. 2004) is an example of a somewhat milder *r*-element enhancement.

Many of the key neutron-capture elements in these stars are observable from the ground, such as Eu, Gd, and Dy and more recently Os, Ir, Pb, Th and U (Cayrel et al. 2001; Hill et al. 2002; Sneden et al. 2003; Plez et al. 2004). However, observations with HST/STIS are crucial to obtain abundances of those elements that have no measurable lines in the visible domain (see also Cowan et al. 2005). These include the heaviest third-peak elements such as Pt, Au, and Bi. Abundances of first- and second-peak elements from near-UV lines in the same STIS spectra will be presented in a forthcoming paper.

3. Observations

CS 31082-001 was observed with the Space Telescope Imaging Spectrograph (STIS) in the near UV (program ID 9359; PI: R. Cayrel). STIS spectroscopic mode E230M combines an échelle grating with a NUV-MAMA detector to obtain spectra in the wavelength range 1575–3100 Å, at a resolution of $R = 30\,000$. Achieving $S/N \sim 40$ in this mode required 45 orbits, but pointing problems caused the spectra of some visits to be of much lower quality, and they were discarded.

Reductions were performed using the STIS pipeline and included the most up-to-date scattered light routines developed at STScI. Co-added and rectified spectra were obtained with the IRAF tasks "scombine" (average mode) and "continuum", which were applied to the high quality spectra only (sequential visit numbers 2, 3, 5, 51, 54, 6, 10). The mean spectra have good $S/N \approx 40$ in the range 2600–3070 Å, comprising orders 2 to 13.

4. Abundance determination from the STIS spectra

The third n-capture peak comprises the elements with $76 \leq Z \leq 83$, including Os, Ir, Pt, Au, Pb and Bi. These elements can be produced in both the slow and rapid neutron-capture processes, although in metal-poor stars the r-process is expected to be the dominant production channel (Truran 1981). The actinides with $Z \geq 89$ include the purely r-process radioactive elements Th and U, already observed in the visible region.

4.1. Identification of lines

Given that CS 31082-001 exhibits an r-process element pattern which may be different from that of other r-II stars, we computed synthetic spectra for all lines of the elements Os, Ir, Pt, Au, Pb, Bi, Th and U from the VALD database, with different enhancement factors, in order to identify useful lines. All lines were checked for proper intensities and possible blends, and lines with major and/or uncertain blends were rejected.

The most reliable lines retained are reported in Table 1; for Bi we kept all three available lines for further checking.

4.2. Placing the continuum

We employ the spectrum synthesis code Turbospectrum (Alvarez & Plez 1998), which accounts properly for scattering in the continuum, a major effect in the UV (Cayrel et al. 2004). The importance of taking scattering in the continuum into account is illustrated in Fig. 1 for the region of the Pb I line at 2833 Å. The spectrum was computed alternatively by including all continuum opacity into the absorption coefficient, while the line absorption was not modified. The computed lines become weaker in the latter case, substantially overestimating the abundances needed to match the observed spectrum.
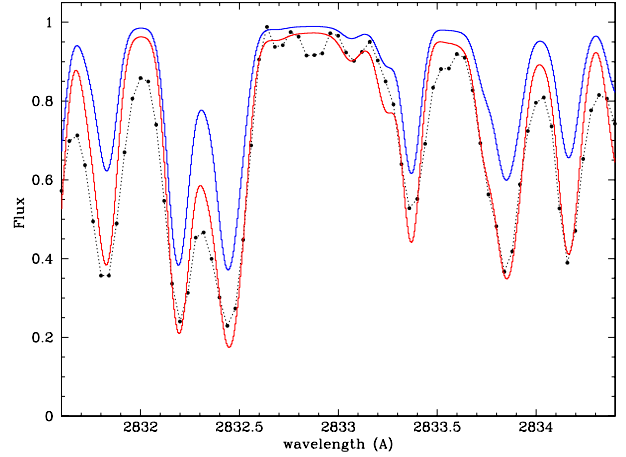
Fig. 1. Observed HST/STIS spectrum (dots) with synthetic spectra including scattering in the continuum as in Turbospectrum (red line) or with all continuum opacity (scattering and absorption) included in the absorption coefficient (blue). The lines remain in pure absorption.
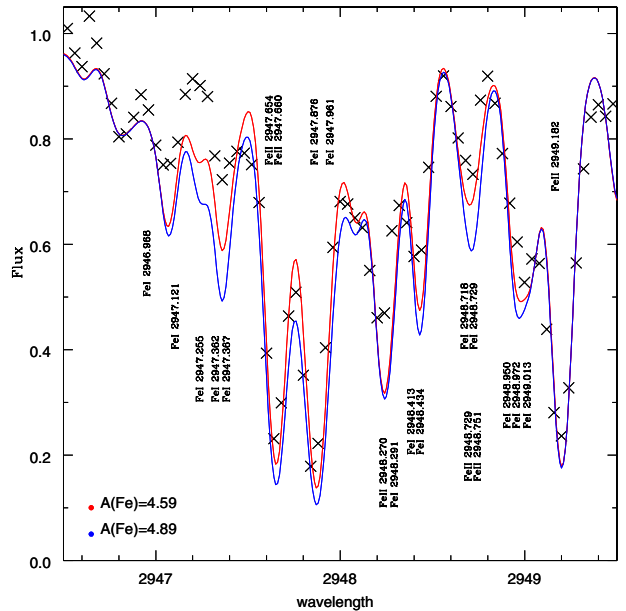
Fig. 2. Fe I lines in the HST/STIS spectrum of CS 31082–001(crosses) compared with synthetic spectra for [Fe/H] = −2.9 as determined from our optical spectra (red line) vs. a spectrum for [Fe/H] = −2.6 (blue line).

This effect was discussed in great detail by Hayek et al. (2011) in the context of 3D models of metal-poor red giant stars. Thus, treating continuum scattering in absorption would result in larger Fe abundances from these UV lines. To further check our computations of the UV spectrum, we used a series of Fe I lines. As shown in Fig. 2, the Fe abundance derived from our exquisite optical spectra ([Fe/H] = −2.9; Hill et al. 2002) also fits the UV lines very well.

4.3. Abundance determination

The present abundance determinations are based on the OSMARCS LTE model atmospheres (Gustafsson et al. 2003). The stellar parameters are adopted from Hill et al. (2002): $T_{\rm eff} = 4825$ K, $\log g = 1.5$, [Fe/H] = −2.9, and $v_{\rm t} = 1.8$ km s^{-1}.

Table 1. Adopted spectral lines, oscillator strengths with references, and abundances in CS 31082-001.

λ(Å)	χ_{ex} (eV)	$\log gf$	Ref.	$\log \epsilon(X)$
	Bi I $Z = 83$			
2989.018	1.416	**0.710**	1	–0.5
3024.635 (order 3)	1.914	**1.350**	1	+0.2
3024.635 (order 2)	1.914	**1.350**	1	–0.3
3067.707	0.000	**0.220**	1	–0.4
	Pb I $Z = 82$			
2833.053	0.000	**–0.670**	2	–0.65
		–0.580	3	
	Au I $Z = 79$			
2675.937	0.000	**–0.450**	4	–1.0
	Pt I $Z = 78$			
2771.660	0.096	–1.130	5	
		–1.080	6	+0.40
2929.789	0.000	–0.800	7	
		–0.700	6	+0.20
	Ir I $Z = 77$			
2758.223	0.717	**–1.670**	8	+0.40
2904.807	0.881	**–1.160**	8	+0.20
2924.792	0.000	**–0.661**	9	–0.30
3047.158	1.623	**–0.500**	8	+0.40
	Os I $Z = 76$			
3058.655	0.000	–0.430	10	
		–0.410	11	–0.07

**Notes.** The adopted oscillator strengths are shown in bold face.

References. 1: Andersen et al. (1972); 2: Penkin et al. (1963); 3: Biémont et al. (2000); 4: Hannaford et al. (1981); 5: Gough et al. (1982); 6: Den Hartog et al. (2005); 7: Lotrian et al. (1982); 8: Corliss & Bozman 1962; 9: Xu et al. (2007); 10: Kwiatwski et al. (1984); 11: Quinet et al. (2006).

Table 2. New oscillator strengths for Ir and Au from (1): Xu et al. (2007) and (2): Fivet et al. (2006).

Species	λ(Å)	$\log gf$ (VALD)	$\log gf_{adopted}$	Ref.
Ir I	2694.227	–0.220	–0.100	1
Ir I	2823.179	–1.530	–1.335	1
Ir I	2824.446	–0.870	–0.532	1
Ir I	2836.397	–0.960	–0.883	1
Ir I	2882.633	–1.150	–1.130	1
Ir I	2924.792	–0.650	–0.661	1
Ir I	2934.631	–0.590	–0.513	1
Ir I	2936.689	–1.030	–1.057	1
Ir I	2943.153	–0.430	–0.343	1
Ir I	2951.216	–1.520	–1.831	1
Ir I	2974.098	–2.770	–2.254	1
Ir I	2980.649	–1.170	–1.723	1
Ir I	2985.806	–1.570	–1.163	1
Ir I	2996.081	–1.660	–1.701	1
Ir I	3049.435	–1.440	–1.453	1
Ir II	2833.241	+1.924	–0.705	1
Au I	2748.251	–0.360	–1.030	2

In calculating the synthetic spectra, we adopted the reliable element abundances determined from our VLT/UVES spectra by Hill et al. (2002), Cayrel et al. (2004), and Spite et al. (2005). The calculations used the Turbospectrum molecular line lists (Alvarez & Plez 1998) together with the atomic line lists from the VALD database (Kupka et al. 1999), unless updated oscillator strengths were available in the literature (see Tables 1, 2).

The VALD atomic data for many transitions of Ru I and Ta I give too strong lines, and new laboratory oscillator strengths are
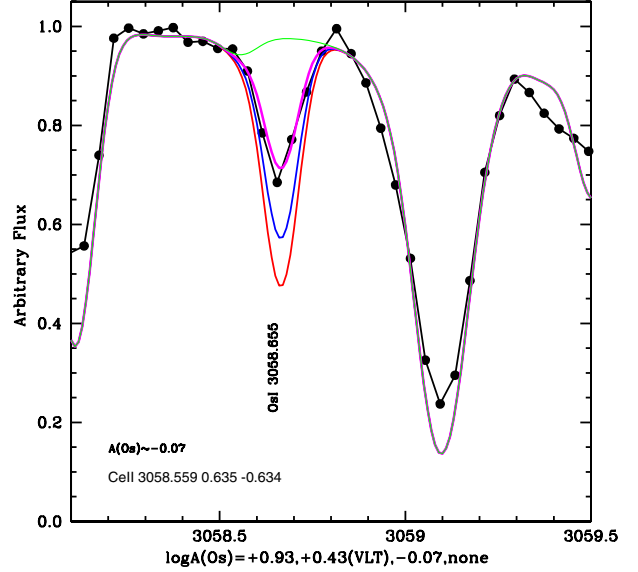
Fig. 3. The Os line at 3058 Å computed for A(Os) = +0.93 (red line), +0.43 (VLT result; blue), –0.07 (magenta), and no Os (green). Black dots: Observed spectrum. A blending line is reported in the figure panel.

needed. We have set [Ru/Fe] = [Ta/Fe] = –5.0 in order not to be disturbed by these spuriously strong lines.

The instrumental resolution at 2700 Å (*FWHM* $\sim$ 0.02 Å) was checked from the spectrum of the comparison thorium lamp. The resolution adopted for the synthetic spectrum calculation, *FWHM* = 0.09 Å or R = 30 800, was based on a fit of the cleanest line, Pb I 2833 Å. The FWHM in the star is higher due to microturbulence in the stellar atmosphere, and probably also due to the orbit of the HST. This resolution was retained in fitting all other lines.

4.3.1. Osmium

From an initial list of 10 Os I lines, only one was used in the final abundance determination (Fig. 3; Table 1). The result, A(Os) = –0.07, is only marginally consistent with that by Hill et al. (2002) from the VLT/UVES spectra (A(Os) = +0.43). We adopt a mean of these two values, namely A(Os) = +0.18.

4.3.2. Iridium

Several Ir I lines are available in the region. We used the atomic data from VALD with oscillator strengths from Xu et al. (2007) (Table 2). No suitable $\log gf$ for the Ir II line at 3042.553 Å was found in the literature, so this line was not used.

Our final Ir abundance is the mean of the results derived from the four best lines listed in Table 1; two examples are shown in Fig. 4. The mean abundance is A(Ir) = +0.18 ± 0.17 (s.d. of mean), in good agreement with the value A(Ir) = +0.20 by Hill et al. (2002) from the UVES spectra, which we adopt as more reliable.

4.3.3. Platinum

Pt abundances could be measured from 14 lines. Although they are rather strong, most had to be rejected due to blends. Our final abundance is based on the two lines in Table 1 and Fig. 5, which yield a mean of A(Pt) = +0.30.
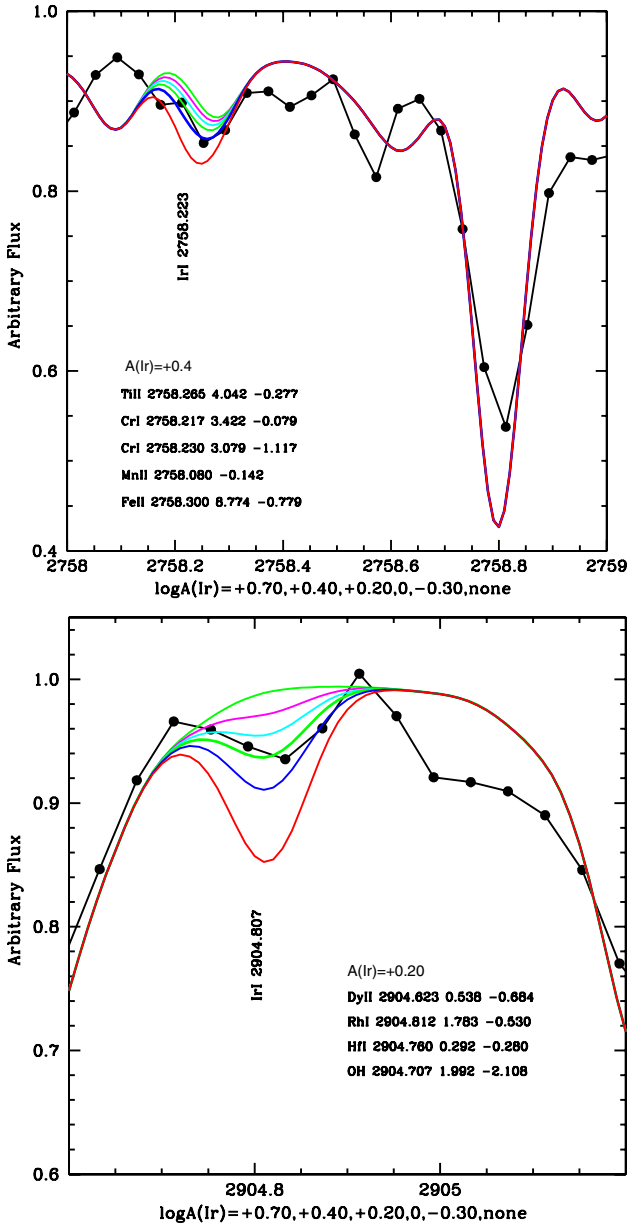
Fig. 4. Ir lines computed for $A(\text{Ir}) = +0.70, +0.40, +0.20, 0.0, -0.30$ and no Ir, respectively (red, blue, green, cyan, magenta and green from bottom). Dots show the observed spectrum; the best fits are for $A(\text{Ir}) = +0.4$ and +0.2. Blending lines are indicated in the figure panels.

4.3.4. Gold

The main abundance indicator is the Au I line 2675.937 Å, which yields $A(\text{Au}) = -1.0$ (Fig. 6). Given the blending and more uncertain continuum definition here, the error in fitting this line is likely higher than for other elements.

We also tried to fit the line Au I 2748.251 Å using the revised log gf from Table 2. The abundance ($A(\text{Au}) \sim -0.8 \pm 0.3$) is compatible with that above, but it was rejected from our final list, as it appears only as an asymmetry in another line.

4.3.5. Lead

The Pb I 2833.053 Å line is shown in Fig. 7; blending by the Fe II 2833.086 Å line (log $gf = -0.483$; Fuhr & Wiese 2006) was taken into account. Plez et al. (2004)
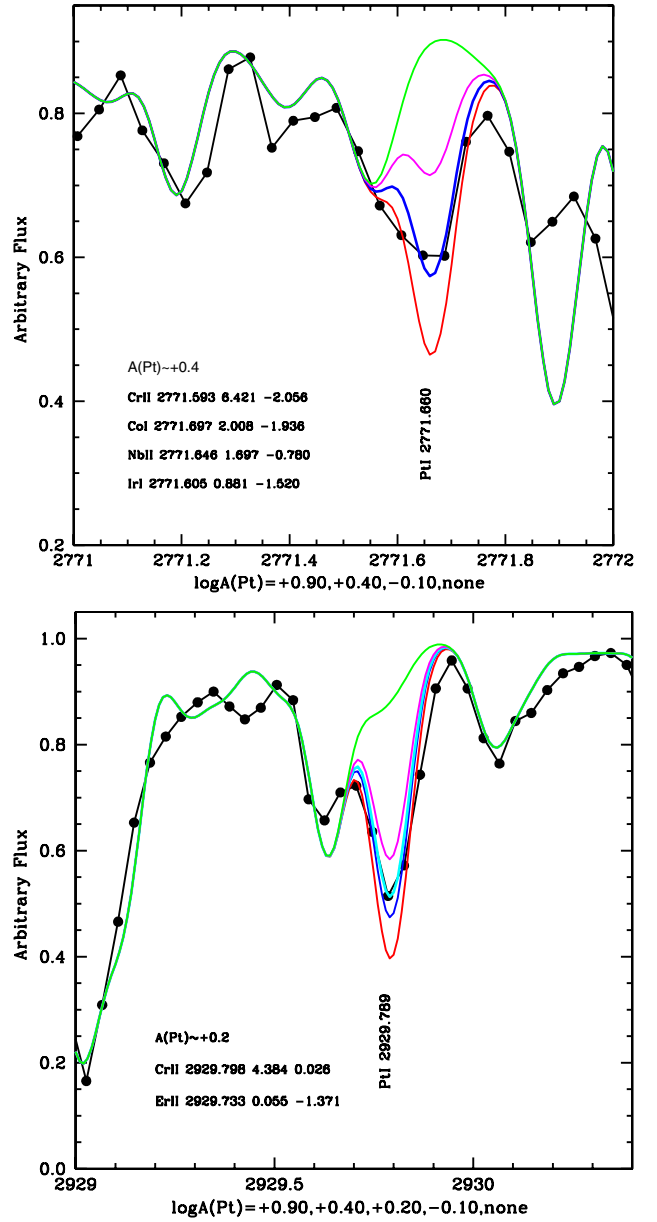

Fig. 5. Pt lines computed for $A(\text{Pt}) = +0.90, +0.40, +0.20, -0.10$ and no Pt. The best fit is for $A(\text{Pt}) = +0.40$ (both lines). Symbols as in Fig. 4.

determined $A(\text{Pb}) = -0.55$ for CS 31082-001 from the Pb I line at 4057.718 Å in a VLT-UVES spectrum with $R \approx 80\,000$ and $S/N \approx 600$/pixel. The stronger line at 2833.053 Å, used here, gives $A(\text{Pb}) = -0.65$, confirming the Pb deficiency pointed out by Plez et al. (2004).

We adopted the lower value of oscillator strength log $gf = -0.67$, because the higher value would yield a Pb abundance even lower, which seems unlikely.

To our knowledge, we see such low Pb abundances (significantly lower than the solar r-process value) only in CS 31082-001 and in HE 1523-0901 (with a hard upper limit; Frebel et al. 2007), both having very low metalicities of [Fe/H] ~ -3. Only upper limits are available for the other r-only stars with similar metalicities, while the measured Pb abundances (relative to, e.g., Eu) for the stars of [Fe/H] $\gtrsim -2$ are in reasonable agreement with the solar r-process value (Aoki & Honda 2008; Roederer et al. 2009; Note that the "solar r-process value" of Pb as residual from the s-process component is highly uncertain, see Goriely 1999).
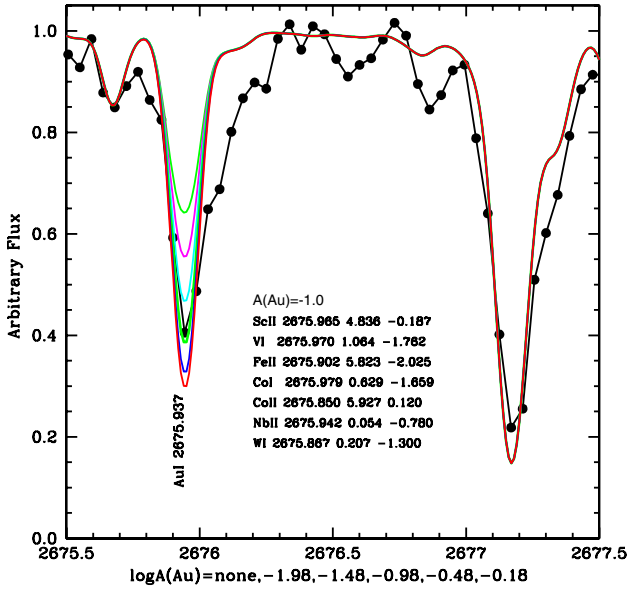
Fig. 6. The Au line computed for $A(\mathrm{Au}) = -0.18$, -0.48, -1.0, -1.48, -1.98, none (bottom to top); the best fit is for $A(\mathrm{Au}) = -1.0$. Symbols as in Fig. 4.
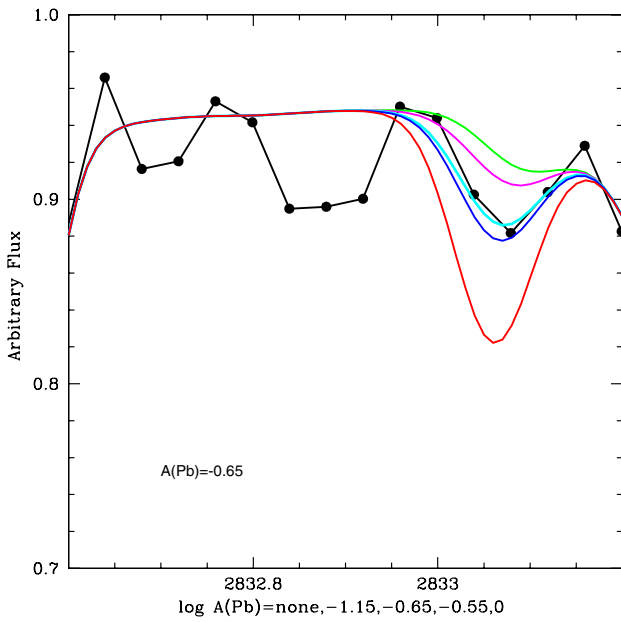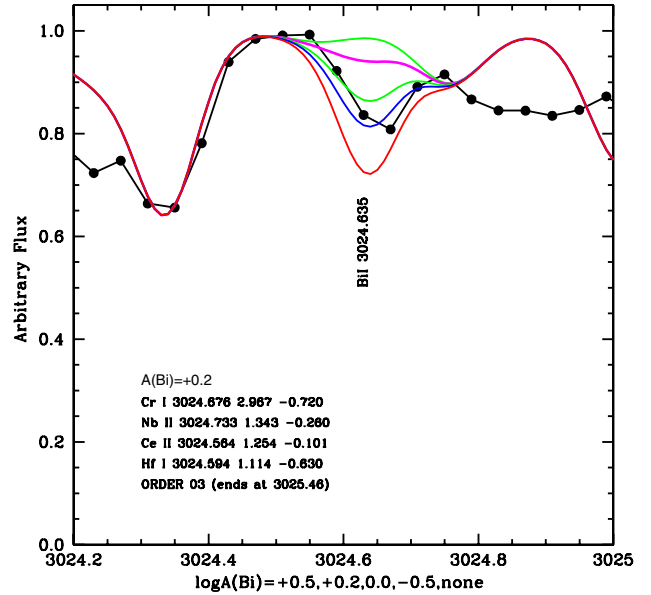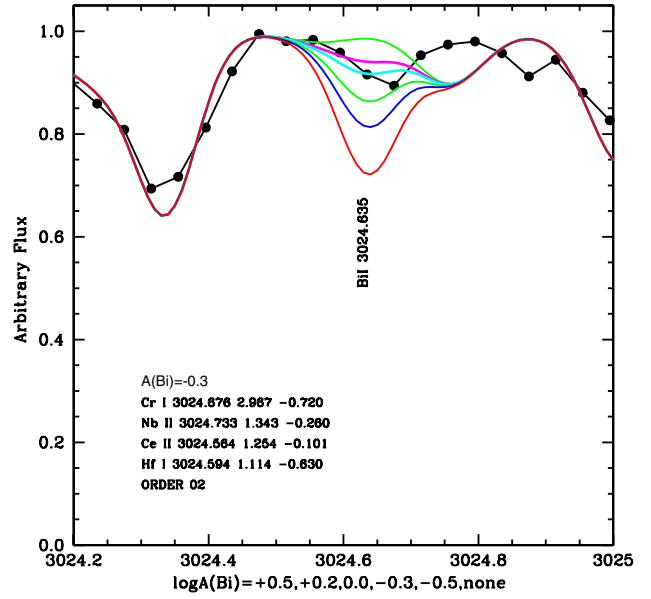

Fig. 7. Lead: Pb line computed with $A(\mathrm{Pb}) = -0.15$, -0.5, -0.65, -1.15, none; the best fit is with $A(\mathrm{Pb}) = -0.65$. Symbols as in Fig. 4.

Fig. 8. The Bi I line at 3024 Å as observed in STIS orders 2 (*upper*) and 3 (*lower*). The synthetic spectra are computed for $A(\mathrm{Bi}) = +0.5$, $+0.2$, 0.0, -0.3, -0.5 and no Bi (*bottom to top*). The best fits are for $A(\mathrm{Bi}) = -0.3$ and $+0.2$, respectively. Symbols as in Fig. 4.

The reason for the presence of these two types (with high and low Pb abundances) is currently unknown. This may not be necessarily associated with the "actinide boost", since the other low-Pb star HE 1523-0901 has a "normal" Th value. Possible reasons could be due to 1) different r-process conditions leading to high and low Pb values (e.g., "hot" and "cold" r-processes; cf. Sect. 5.5) or 2) contaminations from a strong s-process (producing high Pb abundances without others) at metallicities of [Fe/H] ~ -2.

4.3.6. Bismuth

Together with Pb, the Bi abundance is an important calibration point for zero-age *r*-process abundance distribution models,

independent of the uncertain Solar Bi *r*-process abundance (Schatz et al. 2002). Our STIS spectra of CS 31082-001 allow us to determine the first Bi abundance in an *r*-element-rich star; the only other Bi abundance in an EMP star was obtained for an *s*-element rich star by Ivans et al. (2005).

The three most useful Bi I lines at 2989.018, 3024.635, and 3067.707 Å are shown in Figs. 8, and 9. The 3024.6 Å line is present in both STIS échelle orders 2 and 3, but it is closer to the blaze maximum in order 2 and thus has better S/N. The derived abundances are $A(\mathrm{Bi}) = -0.3$ and $+0.2$, respectively, but we consider the former value to be more reliable.

Of the two remaining lines, the abundance from the weak line at 2989 Å is compatible with $A(\mathrm{Bi}) = -0.50$. The Bi I line at 3067.707 Å is heavily blended (Fig. 9), in particular with a strong OH line. Adopting the O abundance by Hill et al. (2002), we derive a Bi abundance for the blended line which is compatible with $A(\mathrm{Bi}) = -0.40$. Given the blends however, we do

Table 3. Solar *r*- and *s*-process fractions (Simmerer et al. 2004) and total Solar abundances of third-peak heavy elements.

El.	Z	Fraction		$\log \epsilon(X)_\odot$						
		r	*s*	(1)	(2)	(3)	(4)	(5)	(6)	(7)
Os	76	0.916	0.084	1.45	1.45	1.25	2.03?	1.40	1.45	**1.36**
Ir	77	0.988	0.012	1.35	1.35	1.38	1.35	1.38	**1.38**	–
Pt	78	0.949	0.051	1.8	1.8	1.64	—	1.62*	**1.74**	–
Au	79	0.944	0.056	1.01	1.01	1.01	—	0.92	**1.01**	–
Pb	82	0.214	0.786	1.85	1.95	2.00	1.75?	1.75	**2.00**	–
Bi	83	0.647	0.353	0.71*	0.71*	0.65	0.09*	0.65*	**0.67***	–
Th	90	1.000	0.000	0.12	0.08*	0.06	0.51?	0.02	<0.08	**0.08**
U	92	1.000	0.000	<−0.47	<−0.47	<−0.47	-0.51	-0.54*	<−0.47	–

References. 1: Anders & Grevesse (1989); 2: Grevesse et al. (1998); 3: Sneden et al. (2008); 4: Hill et al. (2002) and Plez et al. (2004); 5: Asplund et al. (2009); 6: Lodders et al. (2009); 7: Caffau et al. (2011). Adopted abundances from Lodders et al. (2009) and Caffau et al. (2011) are marked in boldface. * Meteoritic abundances.
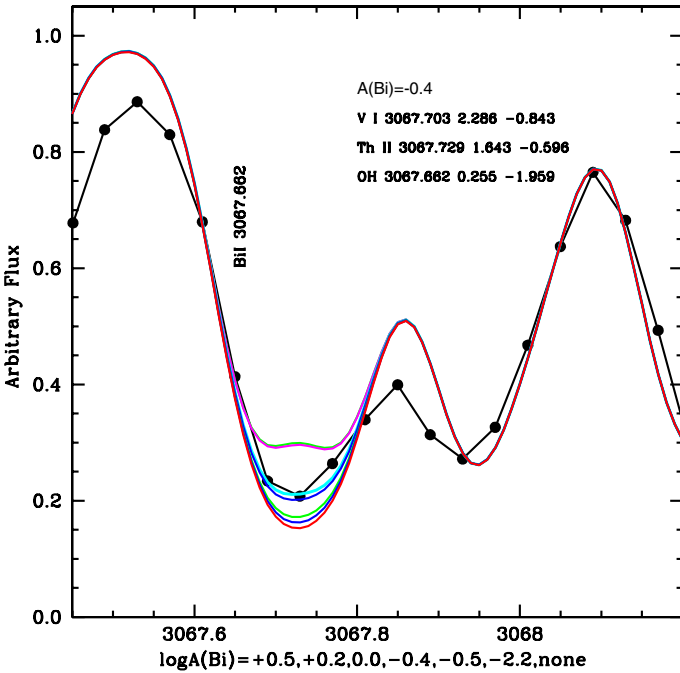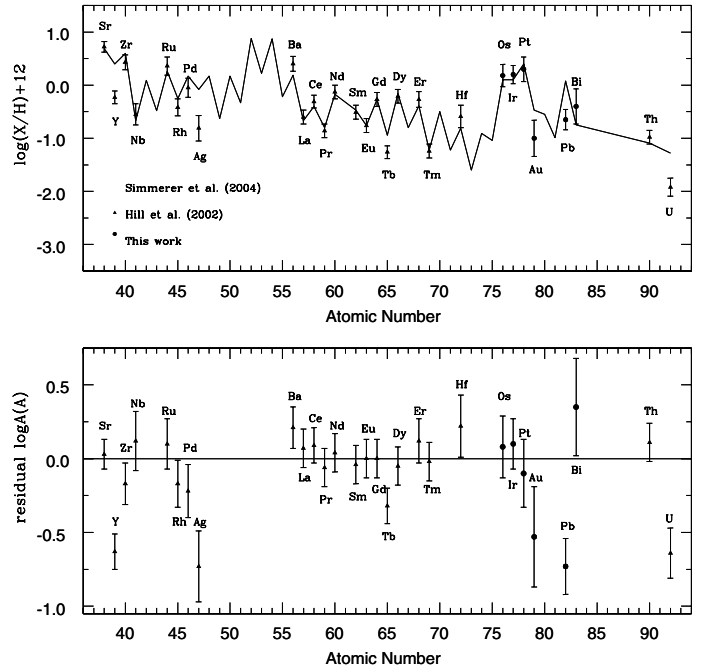

Fig. 9. The Bi I line at 3067 Å computed for A(Bi) = 0.5, 0.2, 0.0, −0.4, −0.5, and −2.2 and none. Symbols as in Fig. 4.

Fig. 10. Solar *r*-process abundance values and residuals from Simmerer et al. (2004) (solid lines, scaled to Eu), compared to the abundances in CS 31082-001.

not give weight to this line. Our higher-resolution VLT/UVES spectrum is very noisy in this wavelength range, but also agrees with the lower abundance. Thus we adopt a mean of results, excluding order 3 for the 3024.635 Å line, giving A(Bi) = −0.4 as our final abundance.

We attribute the possibility of measuring the bismuth abundance to it being probably stronger than in other stars, given the acnitide boost verified for Th and U. A more extensive check on other STIS observed r-process metal-poor stars would be needed to confirm this.

4.3.7. Thorium

Several Th lines appear in our STIS spectra, but all of them are weak and/or blended. Thus we retain the very well-determined Th abundance by Hill et al. (2002), which is based on 8 lines.

4.3.8. Adopted final abundances

Solar abundances and *r*- and *s*-fractions from the literature are compared in Table 3[1].

The final abundances in CS 31082-001 as determined from the VLT/UVES (Hill et al. 2002; Plez et al. 2004) and from our STIS spectra are compared in Table 4. The *r*-element overabundances relative to Solar are given in the last column of the table and are illustrated in Fig. 10.

4.3.9. Uncertainties of the derived abundances

The total error budget of the abundance determination contains the effects of errors in the adopted stellar parameters as well as the observational uncertainties. Abundance changes corresponding to $+1\sigma$ errors of the fundamental stellar parameters adopted by Hill et al. (2002): $\Delta T_{\text{eff}} = +50$ K, $\Delta \log g = +0.3$, $\Delta v_{\text{t}} = +0.2$ km s^{-1} and their sum are reported in Table 5.

---

[1] We adopt the notation $A(X) = \log \epsilon(X) = \log n(X)/n(H) + 12$, with n = number density of atoms.

Table 4. Abundances in CS 31082-001 as derived from our VLT spectra (Hill et al. 2002; Plez et al. 2004), from HST/STIS (present paper), and our adopted final abundances.

Element	Z	$\log \epsilon(X)_\odot$	$\log \epsilon(X)_*$ VLT	$\log \epsilon(X)_*$ HST	$\log \epsilon(X)_*$ adopted	$\log [X/Fe]_*$ adopted
Os	76	+1.40	+0.43	–0.07	+0.18	+1.72
Ir	77	+1.38	+0.20	+0.18	+0.20	+1.72
Pt	78	+1.62	–	+0.30	+0.30	+1.46
Au	79	+0.92	–	–1.00	–1.00	+0.89
Pb	82	+1.75	-0.55	-0.65	-0.65	+0.25
Bi	83	+0.71	–	–0.40	–0.40	+1.83
Th	90	+0.17	-0.98	–	–0.98	+1.84
U	92	–0.07	-1.92	–	–1.92	+1.68

Table 5. Error budget for the final abundances.

Species	$\Delta(T_{eff})$	$\Delta(\log g)$	$\Delta(v_t)$	$\Delta(T,g,v_t)$	Δ_{obs}	Δ_{Tot}
Os I	+0.050	–0.002	–0.015	0.050	0.05	0.07
Ir I	–0.050	+0.002	–0.001	0.053	0.05	0.07
Pt I	+0.100	+0.002	–0.200	0.225	0.05	0.23
Au I	–0.200	–0.100	–0.200	0.280	0.20	0.34
Pb I	+0.100	+0.150	+0.010	0.180	0.05	0.19
Bi I	–0.150	–0.002	–0.001	0.150	0.30	0.33
Th II	0.048	0.090	–0.008	0.132	0.020	0.13
U II	0.046	0.093	–0.002	0.131	0.110	0.17

Notes. $\Delta(T_{eff})$ etc. are the abundance changes corresponding to $+1\sigma$ changes in each of the three stellar parameters, and their sum; Δ_{obs} combines the observational uncertainties discussed in the text, and Δ_{Tot} is the total error estimate for each element.

Observational errors (Δ_{obs}) include the uncertainties in defining the continuum, fitting the line profiles, and in the oscillator strengths. Combining all of these terms leads to the total error estimates (Δ_{Tot}) reported in Table 5.

4.3.10. Previous data

Bi was previously measured only in the *s*-process rich star CS 29497-030 (Ivans et al. 2005), while Au was measured in BD+17 3248 by Cowan et al. (2002). This measurement is also shown in Sneden et al. (2008) – see their Figs. 10, 11 with error bars; in their Table 2 they give $\log \epsilon(Au) = -0.9$ for this star.

Pt and Os were first detected in HST spectra of HD 126238 ([Fe/H] = -1.7) by Cowan et al. (1996), using the lines Pt I 2929.79, 3064.71, Os I 2838.61, 3058.05 Å. Upper limits on Pb from the lines Pb I 2833, 3683 and 4058 Å were also given.

5. Radioactive chronometry from Uranium and Thorium

5.1. Background

Radioactive isotope dating techniques are in widespread use in geology and archaeology, with ^{14}C as the most notable example. For estimating the billion-year ages of disk and halo stars, Th and U are the only useful elements, and the Th/Nd abundance ratio as a galactic chronometer was pioneered by Butcher (1987). Later investigations preferred the pure *r*-process element Eu as the stable reference, as half of the Nd abundance in the Solar system is due to the *s*-process. However, a basic obstacle to the use of ^{232}Th as a chronometer is its long half-life (14.6 Gyr), which severely limits the attainable observational precision. A

more fundamental difficulty is to estimate the initial production ratio of *r*-process elements belonging to the separate second and third neutron-capture peaks.

The ages of EMP stars ([Fe(H) ≤ -3) are of particular interest: such stars could have formed in the very earliest epoch of star formation, corresponding to redshifts at least $z > 3$, and more probably $z > 10$, higher than directly observed from the highest spectroscopic redshift of $z = 8.6$ (Lehnert et al. 2010), and provide a hard lower limit to the age of the Universe. The detection of not only Th, but also – for the first time – U in CS 31082-001 by Cayrel et al. (2001) and Hill et al. (2002) opened the way to more accurate radioactive cosmochronometry: the 4.6-Gyr half-life of ^{238}U – thus an 8-fold decay during a Hubble time – allows a much more precise measurement of the age. All the heaviest neutron-capture elements would thus have formed essentially simultaneously under near-identical conditions, even prior to the formation of CS 31082-001 itself, and provide stable references for the decay of Th and U.

Because of the large "actinide boost" discovered in CS 31082-001, Eu and other second-peak elements cannot be used resulting even in negative ages from the Th chronometer, however, and even such third-peak elements as Os or Ir gave ambiguous results. This led Cayrel et al. (2001) and Hill et al. (2002) to adopt the U/Th ratio as the most reliable chronometer: Although the slow decay of Th leads to a larger formal uncertainty, as seen from the following relations (Cayrel et al. 2001),

$$\Delta t(Gyr) = 46.7[\log(Th/r)_{init} - log(Th/r)_{now}]$$
$$\Delta t(Gyr) = 14.8[\log(U/r)_{init} - log(U/r)_{now}]$$
$$\Delta t(Gyr) = 21.8[\log(U/Th)_{init} - \log(U/Th)_{now}]$$

the systematic errors are much reduced because both the atomic and nuclear structures of Th and U are very similar: most errors in the atmospheric parameters of the star cancel out in the observational determination of the abundance ratio U/Th, and many systematic errors in the initial production ratio of two nuclei with similar masses cancel out as well, as stressed by e.g. Goriely & Clairbaux (1999), Truran (2001) or Cowan et al. (2005). The formal error in the radioactive cosmo-chronometry has been discussed in detail by Ludwig et al. (2010) who provide a ready to use formula relating the error on age to the errors in abundance determination. The formula is applicable also to the case of the ratio of two radioactive elements, provided the lifetime is replaced by the harmonic mean of the lifetimes of the two elements.

The Cayrel et al. (2001) and Hill et al. (2002) age determination of 13.4 ± 3.3 Gyr for CS 31082-001 is thus independent of galactic chemical evolution and stellar internal structure theory, and has already been applied in tests of cosmological models, e.g., Ferreras et al. (2001).

In the following, we examine the reliability of the Th and U chronometers with the variety of heavy reference elements now available, including our new results for Pt and Au. Our new abundance determinations for the daughter elements Bi and Pb – the decay products of Th and U – also provide a valuable cross-check of the results. As noted above, Frebel et al. (2007) identified a second star, HE 1523-0901, in which U and Th could be measured and several chronometer ratios could be compared, as this star exhibited no actinide boost, but this star does not (yet) possess the additional data presented here for CS 31082-001.

Table 6. Computed production ratios (PR) of U vs. some stable *r*-process elements and Th, observed abundance ratios, and age estimates.

Chrono. pair	PR	log (PR)	Ref.	CS 31082-001 log (U/X)	Age (Gyr)
U/Os		−1.37	1	−2.10	10.8
		−0.70	3		20.7
U/Ir		−1.40	1	−2.12	10.7
	0.05036	−1.298	2		12.2
		−1.13	3		14.7
U/Pt	0.013	−1.886	2	−2.22	5.0
		−1.57	3		9.6
U/Th		−0.22	1	−0.94	15.7
	0.556	−0.256	2		14.9
		−0.29	3		14.2
	0.50**	−0.30	4		13.95

References. 1: Schatz et al. (2002); 2: Cowan et al. (2002); 3: Wanajo et al. (2002) with initial electron fraction $Y_e = 0.40$; 4: Goriely & Arnould 2001; ** the value used by Hill et al. (2002).

5.2. Chronometers based on U/Os, Ir, Pt and Au ratios

Radioactive chronometer ages based on the observed abundances of a series of third-peak *r*-elements, including Os, Ir, Pt, Au, Bi, Pb, Th and U, and earlier estimates of the theoretical production ratios (PRs) are listed in Table 6 (new PRs for Au are reported in Table 7). As seen, the dispersion in the results is large, except for the U/Th ratio as noted above.

We discuss the uncertainties of these ages in the following. The total errors in the observed element abundances were summarised in Table 5, but we note that the error in the observed U/Th ratio is in fact only 0.11 dex (Hill et al. 2002, Table 6), due to the compensating factors discussed above. Hence, the dominating uncertainties are due to the nuclear-physics calculations of the initial productions ratios of the elements listed here, which we discuss in the following sections.

5.3. Computed element production ratios

Production ratios were computed for a variety of astrophysical sites with a variety of nuclear input data (Goriely & Arnould 2001; Cowan et al. 2002; Schatz et al. 2002; Wanajo et al. 2002). The uncertainties in the U/Th ratio arising from the astrophysical site modelling are very small (Wanajo & Ishimaru 2006); thus, the errors are mostly due to uncertainties in the nuclear data.

For the other elements, site-independent calculations (Goriely & Arnould 2001; Schatz et al. 2002; Cowan et al. 2002), which fit parameterised models to observed abundance curves for the third-peak elements, cannot in principle provide error estimates for the Production Ratios (PRs) of themselves. To get a representative estimate of the uncertainties from astrophysical modelling, we have therefore simply taken the differences of the results from the cold and hot models of Wanajo (2007; see below).

Table 7 lists the PRs and derived ages from the "hot" and "cold" nucleosynthesis calculations of Wanajo (2007), which are based on SN neutrino wind models with updated nuclear input data (based on the HFB-9 model of Goriely et al. 2005) and revise the older calculations by Wanajo (2002). The cold *r*-process can be realized in rapidly expanding outflows in which the temperature quickly decreases below $<5 \times 10^8$ K before the formation of the third-peak *r*-process elements ($A \sim 195$). This condition may be associated with low-mass supernovae (Wanajo 2007) or binary neutron star mergers (Wanajo & Janka 2011).

However, these calculations are not designed for age determinations (i.e., with no detailed fit to stellar abundances). More seriously, there are problems in the Th and U abundances originating from the erroneous nuclear data for $A > 240$ (see footnote 2 in Wanajo 2007). We discuss the different production models below.

5.4. Ages from U referred to Os, Ir, Pt and Au

As shown in Table 6, some of the PRs reported there lead to reasonable age estimates, while others (e.g. from U/Os or U/Pt) are very discrepant. Ages from the U/Th ratio are much more consistent, as noted earlier.

Comparing with Table 7, Wanajo et al. (2002) and Wanajo (2007) derive too high ages from the U/Os, U/Ir and U/Pt ratios, although a comparison with the abundances of CS 31082-001 in Fig. 3 of Wanajo (2007) did show good consistency. The age from U/Au is uncertain because our abundance determination for Au is based on just a single line. On the other hand, the ages from U/Au, U/Pb and U/Bi, in particular for the cold *r*-process model with low Pb abundances, are quite reasonable. Again, the U/Th chronometer gives the most robust results.

5.5. Consistency of the U, Th, Bi and Pb age indicators

Apart from any direct *r*-process production, Pb and Bi originate predominantly as α-decay products from the actinides with $A \geq 210$, which are co-produced with Th and U. This indicates that Th/Pb, Th/Bi, U/Pb and U/Bi should serve as more reliable chronometer pairs than those involving the lighter elements, such as Os, Ir, Pt or Au, except for U/Th.

Nevertheless, most nucleosynthesis predictions for Pb and Bi (Goriely & Arnould 2001; Cowan et al. 2002; Schatz et al. 2002; Wanajo et al. 2002) show substantially higher Pb abundances than actually observed in CS 31082-001. This inconsistency becomes larger when including the products from the α-decay of the known amounts of Th and U in the Pb abundance (Plez et al. 2004).

As detailed in Plez et al. (2004), the total Pb abundance is the sum of any assumed initial *r*-process Pb production plus the radioactive decay products of Th and U. Thus, ^{238}U decays into ^{206}Pb, ^{232}Th into ^{208}Pb, ^{235}U into ^{207}Pb, while an unknown amount of ^{234}U may decay into ^{206}Pb. In CS 31082-001, the decay of ^{238}U, ^{232}Th and ^{235}U leads to log ϵ(Pb) = −0.59, adopting the most likely stellar parameters (see Plez et al. 2004). The interpretation was that the observed value of log ϵ(Pb) = −0.55 would leave little if any room for an initial *r*-production of Pb. Our improved value from the STIS spectra of log ϵ(Pb) = −0.65 confirms and reinforces this conclusion, i.e. that little if any Pb was produced prior to the formation of CS 31082-001. What is seen now is due to the decay of the original content of Th and U, the rest of which we can also observe today.

On the theoretical front, the results by Wanajo (2007) showed that a low initial production of Pb, compatible with the amount seen in CS 31082-001 (Plez et al. 2004), can be explained by a "cold" *r*-process in a low-temperature environment ($<5 \times 10^8$ K). The robustness of this low Pb production in such low temperature environments should be tested with different astrophysical models as well as with different nuclear data inputs in future works. This is however the only work showing such a low Pb abundance, and we thus compare the results by Wanajo (2007) for the cold model (with a final constant temperature of $T_f = 0.1 \times 10^9$ K) with those for the hot model ($T_f = 1.0 \times 10^9$ K).

Table 7. Production ratios (PR) of U vs. the stable *r*-process elements and Th, with ages computed from the Wanajo ([2007](#)) hot ([a]) and cold ([b]) models.

Chrono. pair	log (PR) hot,cold	Errors log (PR)	CS 31082-001 log(U/X)	Errors log(U/X)	Age (Gyr)	Errors on ages (Gyr) from PRs	from analysis
U/Os	-0.70^a, -0.80^b	0.10	-2.10	0.16	20.7^a, 19.2^b	1.35, 1.35	2.4, 2.4
U/Ir	-0.89^a, -0.90^b	0.01	-2.12	0.16	18.2^a, 18.1^b	0.2, 0.15	2.4, 2.4
U/Pt	-0.99^a, -1.06^b	0.07	-2.22	0.16	18.2^a, 17.2^b	1.1, 1.1	2.4, 2.4
U/Au	-0.33^a, -0.22^b	0.11	-0.92	0.29	8.7^a, 10.4^b	1.7, 1.7	4.3, 4.3
U/Pb	-0.67^a, -0.36^b	0.31	-1.27	0.09	8.9^a, 13.5^b	5.6, 5.5	1.4, 1.4
U/Bi	-0.55^a, -0.41^b	0.06	-1.52	0.08	14.5^a, 16.4^b	0.8, 0.7	1.2, 1.2
U/Th	-0.30^a, -0.30^b	–	-0.94	0.11	$14.0^{a,b}$	–	–

Notes. Errors on the PRs correspond to $\log(PR^a) - \log(PR^b)$. Both models assume $\log(U/Th) = -0.30$.

Table [7](#) lists the PRs and resulting ages for CS 31082-001 with various chronometer pairs for the hot and cold models in Wanajo ([2007](#)).

Because of the problems in the nuclear data applied (for $A > 240$), only the sums of Th and U abundances are provided directly in Wanajo ([2007](#)). We therefore assume log U/Th = -0.30, which leads to an age of 14.0 ± 2.4 Gyr for CS 31082-001 (Hill et al. [2002](#)), consistent with the age of the Universe of 13.7 ± 0.13 Gyr obtained from cosmological models based on the WMAP data (Spergel et al. [2003](#)). Ages from the pairs U/Pb and U/Bi with the cold model are also reasonably consistent with that from U/Th. This implies that the cold *r*-process can provide consistent explanations for the ages from U/Pb, U/Bi, and U/Th with a low initial Pb value, compatible with that observed in CS 31082-001.

5.6. Comments on different models

The production ratios given in Tables [6](#) and [7](#) are derived from different assumptions: many of the theoretical predictions are based on the classical *waiting point* approximation, in which Fe seeds are bombarded in (n, γ)–(γ, n) equilibrium with a neutron exposure of chosen neutron density, temperature and duration τ (e.g. Schatz et al. [2002](#); Kratz et al. [2007](#)). This classical *r*-process model is able to fit the Solar *r*-process isotopic abundance pattern from Fe to Pb with only four free parameters, which suggests that this method may reflect the general physical properties of the *r*-process site(s).

For the nuclear physics itself, Cowan et al. ([2002](#)) adopted the predicted initial abundance ratios based on an extended Thomas-Fermi model with quenched shell effects far from stability (ETFSI-Q) and a finite-range droplet model with microscopic shell corrections (FRDM+HFB) model (see also Cowan et al. [1999](#)). Goriely & Arnould [2001](#) used a multi-event model in order to find the best astrophysical conditions, considered as free parameters, that would fit a given abundance distribution for a given nuclear input. The yield from each event was not calculated under the waiting-point approximation, but a solution of the full reaction network was made.

Finally, as described above, the Wanajo et al. ([2002](#)) model is based on the neutrino wind scenario arising in a core-collapse supernova. Wanajo ([2007](#)) used the same scenario, but adopting a cold *r*-process which proceeds with competing (n, γ) and β-decays, but without (γ, n) decays when the temperature drops below $\sim 5 \times 10^8$ K. This differs from the traditional (hot) *r*-process at a temperature of $\sim 1 \times 10^9$ K, where the (n, γ)–(γ, n) equilibrium remains a good approximation during *r*-processing.
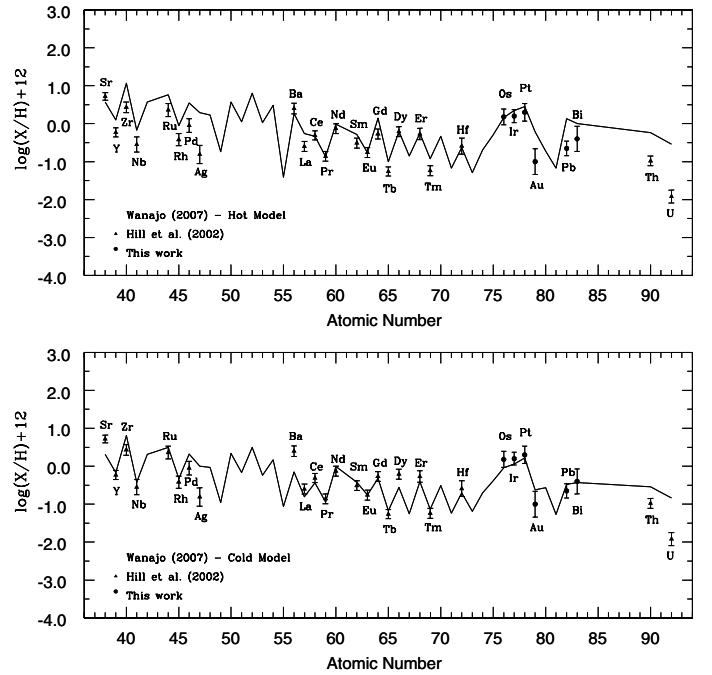

Fig. 11. Predicted abundance patterns for the hot (*upper*) and cold (*lower*) models by Wanajo ([2007](#)), compared with the observed abundances in CS 31082-001.

As Tables [6](#) and [7](#) show, some PRs yield more acceptable ages than others. For example, the Wanajo ([2007](#)) cold model (Table [7](#)) is suitable for both Pb and Bi, whereas the hot model is suitable for Bi, but not for Pb, even though the same U/Th PR is assumed for both models.

Unfortunately, no experimental information is available for the vast majority of the nuclear physics data (Schatz et al. [2002](#)); disagreement between observations and theory would indicate errors in the nuclear data and/or the astrophysical models (or in the observations, of course). Figure [11](#) compares the predictions of the hot and cold models by Wanajo ([2007](#)) with the observed abundances in CS 31082-001, while Fig. [12](#) show the corresponding residuals. The hot model fits many of the second-peak elements well, but fails for the first-peak elements and the heaviest third-peak elements and the actinides. The cold model gives an overall better fit, except for Ba, Os, Dy and a few others. This might suggest that the abundance pattern results from nucleosynthetic processes in several different physical conditions.

Finally, we note that Frebel et al. ([2007](#)) were able to use several different chronometers U/Th, U/Ir, Th/Eu, Th/Eu and Th/Os ratios to derive a more consistent set of ages (~13.2 Gyr) for
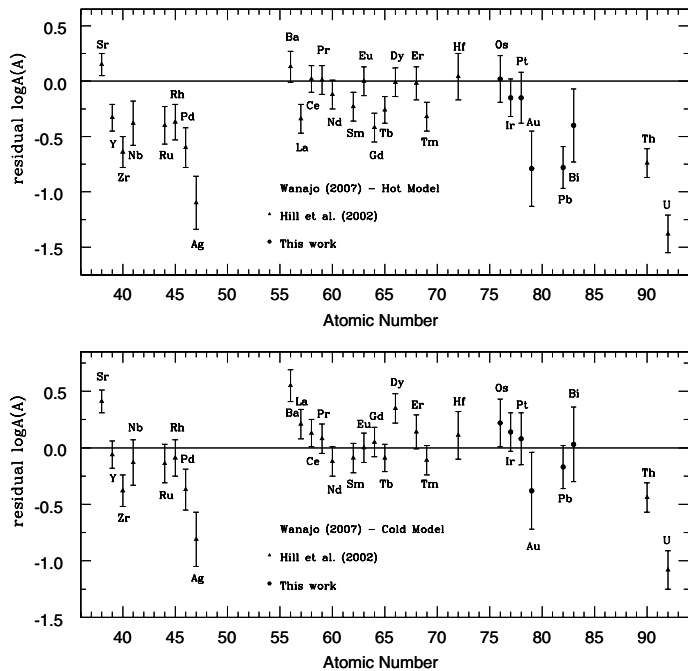
Fig. 12. Abundance residuals of elements in CS 31082-001 from the two Wanajo (2007) model predictions (Fig. 11).

HE 1523-0901 than we find for CS 31082-001. The fact that a strong actinide boost is observed in CS 31082-001, but not in HE 1523-0901, suggests that the production of the heaviest elements in the r-process site(s) may be more complex than revealed so far.

6. Conclusions

For the first time, we have determined abundances for all measurable third-peak elements for an extremely metal-poor r-process enhanced star, including such elements as Pt and Au. The observed abundances ratios in CS 31082-001 should be useful for a better characterisation of the neutron exposure(s) that produced the r-process elements in this star, as well as a guide to improved nuclear data and astrophysical site modelling.

The STIS/HST spectra of CS 31082-001 permitted us to obtain the only abundance determination Bi in a r-II star. Also, the Pb abundance is the unique convincing derivation (others are upper limits), strenghtened by showing agreement between VLT/UVES and STIS/HST data. Combined with a variety of theoretical calculation of the production ratios of the third-peak neutron capture elements and actinides, this allows us to assess the consistency of the results from a number of radioactive chronometer pairs with each other.

The disagreements seen between observation and theory, notably the high ages derived from the U/Os, U/Ir and U/Pt ratios, would indicate that the nuclear data and/or astrophysical modelling are in need of improvement. As Pb and Bi seem to originate primarily from the α-decay of elements with $A \geq 210$, i.e. the actinides co-produced with Th and U, the Th/Pb, Th/Bi, U/Pb and U/Bi ratios may be more reliable chronometers than any others, except for U/Th. Indeed, reasonable ages are found for the "cold" model by Wanajo (2007) from the pairs U/Pb and U/Bi with an adopted age of 14.0 Gyr from the U/Th ratio.

Roederer et al. (2009) found that in most EMP stars with known Pb and Th, the r-process pattern appears to continue to the actinides. The two prime examples, CS 31082-001 and HE 1523-0901, are strikingly different, however, in that Th/Eu ratio

is much higher in CS 31082-001 than the Solar value found in other r-element rich stars. CS 31082-001 also has a very low Pb abundance, consistent with a purely radioactive production of Pb, while only an upper limit, consistent with a Pb deficiency, is available in HE 1523-0901.

We finally comment on the role of the highly r-element enriched stars in the general picture of nucleosynthesis and chemical evolution of the early Galaxy. The binary frequency of these stars is not yet known, but there is at least no observational evidence to suggest that CS 31082-001 itself is a binary. Assuming this to hold in general, these stars are not only our best guide to understand what went on *inside* the generations of stars that preceded the formation of CS 31082-001 and similar r-element rich stars of [Fe/H] $\lesssim -3$, and which already then synthesised even the heaviest elements in the periodic system. They also highlight the poorly-understood processes that permitted the first stars to enrich the early (high-redshift!) Galaxy in heavy elements up to and including the iron peak in very constant proportions while enhancing a minority of stars in r-process elements by large factors. Understanding the conditions of galaxy formation and evolution at that time will be an interesting challenge.

References

Alvarez, R., & Plez, B. 1998, A&A, 330, 1109
Anders, E., & Grevesse, N. 1989, Geochim. Cosmochim. Acta, 53, 197
Andersen, T., Madsen, O. H., & Sorensen, G. 1972, JOSA, 62, 1118
Aoki, W., & Honda, S. 2008, PASJ, 60, L7
Aoki, W., Beers, T. C., Honda, S., & Carollo, D. 2010, ApJ, 723, L201
Argast, D., Samland, M., Thielemann, F.-K., & Qian, Y.-Z. 2004, A&A, 416, 997
Asplund, M., Grevesse, N., Sauval, A. J., & Scott, P. 2009, ARA&A, 47, 481
Beers, T. C., & Christlieb, N. 2005, ARA&A, 43, 531
Beers, T. C., Preston, G. W., & Shectman, S. 1992, AJ, 105, 1987
Biémont, E., Garnir, H. P., Palmeri, P., Li, Z. S., & Svanberg, S. 2000, MNRAS, 312, 116
Butcher, H. R. 1987, Nature, 328, 127
Burris, D. L., Pilachowski, C. A., Armandroff, T. E., et al. 2000, ApJ, 544, 302
Caffau, E., Ludwig, H.-G., Steffen, M., et al. 2011, Sol. Phys., 268, 255
Cayrel, R., Hill, V., Beers, T. C., et al. 2001, Nature, 409, 691
Cayrel, R., Depagne, E., Spite, M., et al. 2004, A&A, 416, 1117
Corliss, C. H., & Bozman, W. R. 1962, NBS Monograph, 53
Cowan, J. J., & Sneden, C. 2006, Nature, 440, 1151
Cowan, J. J., Sneden, C., Truran, J. W., & Burris, D. L. 1996, 460, L115
Cowan, J. J., Pfeiffer, B., Kratz, K.-L., et al. 1999, ApJ, 521, 194
Cowan, J. J., Sneden, C., Burles, S., et al. 2002, ApJ, 572, 861
Cowan, J. J., Sneden, C., & Beers, T. C. 2005, ApJ, 627, 238
De Donder, E., & Vanbeveren, D. 2004, New Astron. Rev., 48, 861
Den Hartog, E. A., Herd, M. T., Lawler, J. E., et al. 2005, 619, 639
Ferreras, I., Melchiorri, A., & Silk, J. 2001, MNRAS, 327, L47
Fischer, T., Whitehouse, S. C., Mezzacappa, A., et al. 2010, A&A, 517, A80
Fivet, V., Quinet, P., Biémont, É., & Xu, H. L. 2006, J. Phys. B: At. Mol. Opt. Phys., 39, 3587
Frebel, A., Christlieb, N., Norris, J. E., et al. 2006, ApJ, 652, 1585
Frebel, A., Christlieb, N., Norris, J. E., et al. 2007, ApJ, 660, L117
Frebel, A., Collet, R., Eriksson, K., et al. 2008, ApJ, 684, 588
Freiburghaus, C., Rosswog, S., & Thielemann, F.-K. 1999, ApJ, 525, L121
Fuhr, J. R., & Wiese, W. L. 2006, J. Phys. Chem. Ref. Data, 35, 1669
Goriely, S. 1999, A&A, 342, 881
Goriely, S., & Arnould, M. 2001, A&A, 379, 1113
Goriely, S., & Clairbaux, B. 1999, A&A, 346, 798
Goriely, S., Demetriou, P., Janka, H.-Th., Pearson, J. M., & Samyn, M. 2006, Nucl. Phys. A, 758, 587
Goriely, S., Bauswein, A., & Janka, H.-T. 2011, ApJ, 738, L32
Gough, D. S., Hannaford, P., & Lowe, R. M. 1982, J. Phys. B, 15, L431

Grevesse, N., & Sauval, J. 1998, SSRv, 85, 161

Gustafsson, B., Edvardsson, B., Eriksson, K., et al. 2003, in Stellar Atmosphere Modelling, eds. I. Hubeny, D. Mihalas, & K. Werner, ASP Conf. Ser., 288, 331

Gustafsson, B., Edvardsson, B., Eriksson, K., et al. 2008, A&A, 486, 951

Hannaford, P., Larkins, P. L., & Lowe, R. M. 1981, J. Phys. B, 14, 2321

Hayek, W., Wiesendahl, U., Christlieb, N., et al. 2009, A&A, 504, 511

Hayek, W., Asplund, M., Collet, R., & Nordlund, Å. 2011, A&A, 529, A158

Hill, V., Plez, B., Cayrel, R., & Beers, T. C. 2001, in Astrophysical Ages and Time Scales, eds. T. von Hippel, N. Mansel, & C. Simpson, ASP Conf. Ser., 245, 316

Hill, V., Plez, B., Cayrel, R., et al. 2002, A&A, 387, 560

Honda, S., Aoki, W., Kajino, T., et al. 2004, ApJS, 152, 113

Hüdepohl, L., Müller, B., Janka, H.-Th., et al. 2010, Phys. Rev. Lett., 104, 251101

Ishimaru, Y., & Wanajo, S. 1999, ApJ, 511, L33

Ishimaru, Y., & Wanajo, S. 2000, in The First Stars, eds. A. Weiss, T., Abel, & V. Hill (Berlin: Springer-Verlag), 189

Ivans, I. I., Sneden, C., Gallino, R., Cowan, J. J., & Preston, G. W. 2005, ApJ, 627, L145

Kratz, K.-L., Farouqi, K., Pfeiffer, B., et al. 2007, ApJ, 662, 39

Kupka, F., Piskunov, N., Ryabchikova, T., et al. 1999, A&AS, 138, 119

Lai, D. K., Bolte, M., Johnson, J. A., et al. 2008, ApJ, 681, 1524

Lattimer, J. M., Mackie, F., Ravenhall, D. G., & Schramm, D. N. 1977, ApJ, 213, 225

Lehnert, M. D., Nesvadba, N. P.H., Cuby, J. G., et al. 2010, Nature, 467, 940

Lodders, K., Palme, H., & Gail, H.-P. 2009, Landolt-Börnstein – Group VI Astronomy and Astrophysics Numerical Data and Functional Relationships in Science and Technology Volume 4B: Solar System, ed. J. E. Trümper, 4.4., 44

Lotrian, J., & Guern, Y. 1982, J. Phys. B, 15, 69

Ludwig, H.-G., Caffau, E., Steffen, M., Bonifacio, P., & Sbordone, L. 2010, A&A, 509, A84

Mathews, G. J., & Cowan, J. J. 1990, Nature, 345, 491

McWilliam, A., Preston, G. W., Sneden, C., & Searle, L. 1995, AJ, 109, 2757

Meyer, B. S. 1989, ApJ, 343, 254

Nilsson, H., Zhang, Z., Lundberg, H., Johansson, S., & Nordstrom, B. 2002a, A&A, 382, 368

Nilsson, H., Ivarsson, S., Johansson, S., & Lundberg, H. 2002b, A&A, 381, 1090

Penkin, N. P., & Slavena, I. Yu. Yu. 1963, Opt. Spectr., 15, 83

Plez, B., Hill, V., Cayrel, R., et al. 2004, A&A, 428, L9

Prantzos, N. 2006, in Proceedings of the International Symposium on Nuclear Astrophysics – Nuclei in the Cosmos – IX, 25–30 June 2006, CERN, 254.1

Quinet, P., Palmeri, P., Biémont, E., et al. 2006, A&A, 448, 1207

Roederer, I. U., Kratz, K.-L., Frebel, A., et al. 2009, ApJ, 698, 1963

Roederer, I. U., Sneden, C., Lawler, J. E., & Cowan, J. J. 2010, ApJ, 714, L123

Schatz, H., Toenjes, R., Pfeiffer, B., et al. 2002, ApJ, 579, 638

Simmerer, J., Sneden, C., Cowan, J. J., et al. 2004, ApJ, 617, 1091

Sneden, C., & Cowan, J. J. 2001, The 7th Texas-Mexico Conf. on Astrophysics: Flows, Blows and Glows, eds. W. H. Lee, & S. Torres-Peimbert, Rev. Mex. Astron. Astrofis. Ser. Conf., 10, 221

Sneden, C., Preston, G. W., McWilliam, A., & Searle, L. 1994, ApJ, 431, L27

Sneden, C., McWilliam, A., Preston, G. P., et al. 1996, ApJ, 467, 819

Sneden, C., Cowan, J. J., Ivans, I. I., et al. 2000, ApJ, 533, L139

Sneden, C., Cowan, J. J., Lawler, J. E., et al. 2003, ApJ, 591, 936

Sneden, C., Cowan, J. J., & Gallino, R. 2008, ARA&A, 46, 241

Spergel, D. N., Verde, L., Peiris, H. V., et al. 2003, ApJS, 148, 175

Spite, M., Cayrel, R., Plez, B., et al. 2005, A&A, 430, 655

Surman, R., McLaughlin, G. C., Ruffert, M., Janka, H.-Th., & Hix, W. R. 2008, ApJ, 679, L117

Thielemann, F.-K., Hirschi, R., Liebendörfer, M., & Diehl, R. 2010, Lect. Not. Phys., 812, 153

Truran, J. W. 2001, IAU Symp. 204, ed. M. Harwitt, 333

Wanajo, S. 2007, ApJ, 666, L77

Wanajo, S., & Ishimaru, Y. 2006, Nucl. Phys. A, 777, 676

Wanajo, S., & Janka, H.-T. 2011, ApJ, submitted [arXiv1106.6142]

Wanajo, S., Itoh, N., Ishimaru, Y., et al. 2002, ApJ, 577, 853

Wanajo, S., Janka, H.-T., & Müller, B. 2011, ApJ, 726, L15

Woosley, S. E., Wilson, J. R., Mathews, G. J., Hoffman, R. D., & Meyer, B. S. 1994, ApJ, 433, 229

Xu, H. L., Svanberg, S., Quinet, P., Palmeri, P, & Biémont, É. 2007, JQSRT, 104, 52